UC Irvine
UC Irvine Previously Published Works

Title

Implications of a transition in the dark energy equation of state for the H0 and σ8 tensions

Permalink

Journal

ISSN

Authors

Keeley, Ryan E
Joudaki, Shahab
Kaplinghat, Manoj
et al.

Publication Date

DOI

Copyright Information

Implications of a transition in the dark energy equation of state for the H_0 and σ_8 tensions

Ryan E. Keeley, [a,b,1] **Shahab Joudaki,**[c] **Manoj Kaplinghat,**[b] **David Kirkby**[b]

[a]Korea Astronomy and Space Science Institute, Yuseong-gu, 776 Daedeok-daero, Daejeon, Korea

[b]Center for Cosmology, Department of Physics and Astronomy, University of California, Irvine, CA 92697, USA

[c]Department of Physics, University of Oxford, Denys Wilkinson Building, Keble Road, Oxford OX1 3RH, U.K.

E-mail: rkeeley@kasi.re.kr

Abstract. We explore the implications of a rapid appearance of dark energy between the redshifts (z) of one and two on the expansion rate and growth of perturbations. Using both Gaussian process regression and a parametric model, we show that this is the preferred solution to the current set of low-redshift ($z < 3$) distance measurements if $H_0 = 73\,\mathrm{km\,s^{-1}\,Mpc^{-1}}$ to within 1% and the high-redshift expansion history is unchanged from the ΛCDM inference by the Planck satellite. Dark energy was effectively non-existent around $z = 2$, but its density is close to the ΛCDM model value today, with an equation of state greater than -1 at $z < 0.5$. If sources of clustering other than matter are negligible, we show that this expansion history leads to slower growth of perturbations at $z < 1$, compared to ΛCDM, that is measurable by upcoming surveys and can alleviate the σ_8 tension between the Planck CMB temperature and low-redshift probes of the large-scale structure.

---

[1]Corresponding author.

Contents

1 The tensions

The current concordance cosmological model consisting of a cosmological constant (Λ) and cold dark matter (CDM) has been remarkably successful in explaining cosmological observables at both high and low redshift [6, 10, 11, 18, 37]. However, within this ΛCDM model, some tensions between datasets have emerged that merit attention. One is the "H_0 tension", which is a mismatch between the direct measurement of the present expansion rate, or Hubble constant, and the value inferred from observations of the cosmic microwave background (CMB) [10, 55, 56].

The second is the "σ_8 tension", which is a discrepancy between the RMS of the linear matter density field ($\sigma(R, z)$) on $8\,h^{-1}\,\mathrm{Mpc}$ scales at redshift $z = 0$ (σ_8) inferred from the CMB and measured by Sunyaev-Zel'dovich (SZ) cluster counts (e.g. [5, 7, 22]). It should be noted that this tension depends on the adopted calibration of the SZ flux to cluster halo mass [52], which is still uncertain. There are also indications that the value of $S_8 = \sigma_8 \Omega_\mathrm{m}^{0.5}$, where Ω_m is the matter density relative to the critical density today, as measured through weak gravitational lensing tomography is in tension with the inference from the CMB (e.g. [2, 35–37, 40–42, 49, 65, 66]).

In addition to the discordance between the direct measurement of H_0 and the CMB, there is also a discordance between the distances calibrated by them. The supernova (SNe) distances calibrated by the local H_0 measurement do not agree at $z \simeq 0.5$ with the distances inferred from the baryon acoustic oscillation (BAO) feature in the correlation function of luminous red galaxies (LRGs) [19] calibrated by the CMB [13]. One way to bring the SNe and LRG distances into agreement is if the true r_drag is smaller than the value from the ΛCDM fit to the Planck data [13].

Though these disagreements could be due to unknown systematic uncertainties in the measurements, an interesting possibility is that these tensions point to new physics. This point of view has merit because H_0 and σ_8 obtained from the CMB are derived parameters calculated from a model-dependent projection over three orders of magnitude in the scale factor, a. One way to evolve the Universe to low redshift in a manner different from ΛCDM is to relax the requirement that the dark energy is a cosmological constant. Evolving dark energy is often quantified by the Chevallier-Polarski-Linder parametrization [25, 50], but more dramatic changes are possible. For instance, scalar-tensor theories satisfying the LIGO/Virgo bound on the propagation speed of gravitational waves [1] can include a dark energy component with equation of state that varies rapidly with redshift [29, 44].

An alternative possibility is that new physics at or before last scattering gives rise to a larger expansion rate in the early Universe and smaller sound horizon at the drag epoch, r_{drag}, compared to ΛCDM. This shifts the CMB prediction and the low-redshift (BAO) features to better agree with the measured value of H_0 [13, 16, 53]. The difficulty in this strategy comes from the fact that the CMB anisotropies are precisely measured [10]. It is difficult to modify the distance scales away from ΛCDM predictions without spoiling its successful predictions for the temperature and polarization anisotropies [16].

Models with new physics at $z > 1000$ typically add one or more extra degrees of freedom. Three possibilities that have been studied are dark radiation [16], strongly interacting massive neutrinos [48], and early dark energy [53]. By adding extra degrees of freedom, any predictions for low-redshift quantities from these models will be more uncertain relative to the ΛCDM prediction, and currently proposed modifications at $z > 1000$ use this reduction in significance to alleviate the H_0 tension [16, 43, 48, 53]. However, should either the CMB polarization power spectrum or H_0 measurements become more precise while maintaining the same central values, the tension would reemerge.

An appealing aspect of these high-z modifications that lead to smaller r_{drag} is that it can make $z < 1$ distance measurements consistent with each other [13]. Our work in this paper asks the complementary question of how these tensions may be alleviated if the expansion rate at last scattering and r_{drag} are unchanged from the ΛCDM inferences. In this case, the path forward is to explore the uncertainty in the dark energy density evolution. We do so in a model-independent (Gaussian process (GP) regression) framework, and with a parametric model (Transitional Dark Energy (TDE) model) for dark energy evolution. Our approach highlights the interesting possibility of evolving dark energy models that alleviate the H_0 tension and predict a slower growth of structure at late times [41].

2   Model-independent expansion history

We use a GP regression to infer the expansion history of the Universe following the procedure used in our previous work [43, hereafter J18]. The repository for that code is archived here [46]. The present analysis differs from J18 in that we forecast results assuming a precision measurement of the Hubble constant at the 1% level, a remarkable feat that could be achieved in the near future. This may be possible through better calibration of Cepheids with Gaia [33, 56, 57, 62], through a standard siren technique with LIGO and Virgo [24], via Population II distance indicators with Gaia [15], or via strong lensing time-delay measurements by the H0LiCOW collaboration [20].

As in J18, we condition the GP regression using direct measurements of the Hubble distance $D_H(z) = c/H(z)$, as well as indirect constraints on D_H from measurements

of the angular diameter distance $D_A(z) = D_C(z)/(1 + z)$, and the luminosity distance $D_L(z) = (1+z)D_C(z)$, where $D_C(z) = \int_0^z D_H(z)dz$. Throughout this work, we assume spatial flatness. We divide out a fiducial expansion history, D_H^0, based on the best-fit Planck+WP flat ΛCDM cosmology from Ade et al. (2013) [4] (the differences between the 2013 and 2018 Planck results are small, and do not noticeably change the GP regression results) with $H_0 = 67.04 \text{ km s}^{-1} \text{ Mpc}^{-1}$, present matter density $\Omega_m = 0.3183$, present dark energy density $\Omega_{DE} = 0.6817$, effective number of neutrinos $N_{eff} = 3.046$, and one massive neutrino species with mass $m_\nu = 0.06$ eV.

We define a GP for $\gamma(z) = \ln(D_H(z)/D_H^0(z))$ with zero mean and covariance function

$$\langle \gamma(z_1)\gamma(z_2) \rangle = h^2 \exp(-(s(z_1) - s(z_2))^2/(2\sigma^2)), \tag{2.1}$$

where the evolution variable $s(z)$ is taken to be $s(z) = \ln(1+z)/\ln(1+z_*)$, and $z_* = 1090.48$ to match the redshift of last scattering for the Planck+WP best fit. Note that $s(z)$ goes from 0 to 1 as z changes from 0 to z_*. We marginalize over the grid of hyperparameters $\{0.01 < h < 0.2, 0.001 < \sigma < 1.0\}$.
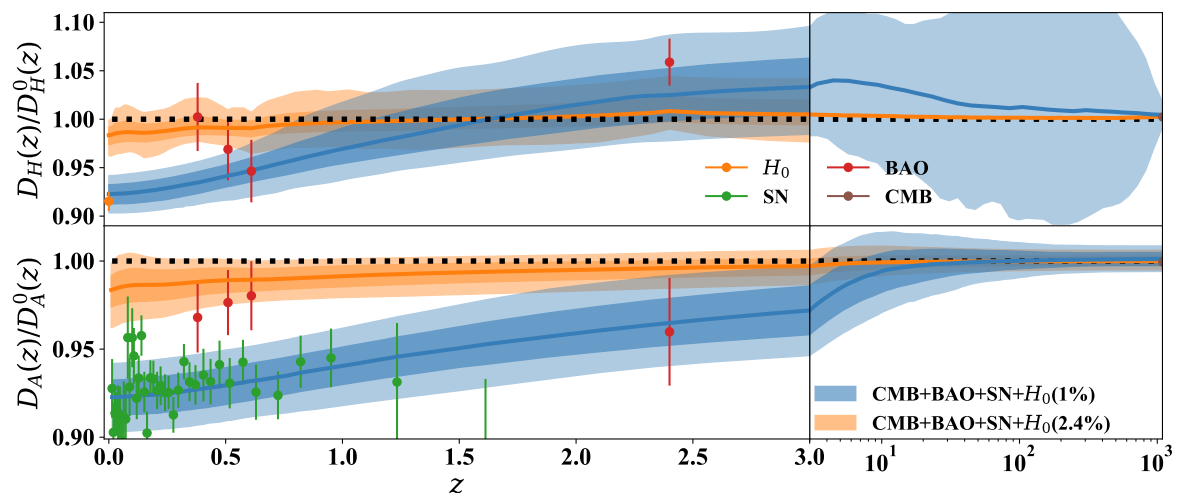
Figure 1. Posteriors for the expansion history as determined by the GP regression (inner 68% and outer 95% confidence levels). The Hubble and angular diameter distances, $D_H(z)$ and $D_A(z)$, are shown in the top and bottom panels, respectively. These distances are shown relative to the fiducial Planck ΛCDM model. The orange shaded regions correspond to the results with the Riess et al. (2016) [56] uncertainty on H_0 as calculated in J18, while the blue shaded regions correspond to forecasts with 1% precision on H_0. The orange and blue solid lines illustrate the median results of the GPs. Note the split linear-logarithmic redshift axis.

We use the following datasets to constrain the GP:

- Planck 2015 CMB temperature and polarization dataset consisting of 'TT', 'TE', 'EE', and 'lowP' angular power spectra [3, 6] which was used to compute the posterior mean and covariance for D_H and D_A at the redshift of last scattering, z_*.

- Distances inferred from the BAO signal encoded in the clustering of LRGs from Beutler et al. (2016) [19].

- Distances inferred from the BAO signal in the auto-correlation of the flux transmission of the Lyα forest and cross-correlation with quasars from Bourboux et al. (2017) [31].

Each of these BAO distances scale with r_{drag}, which we fix to the best-fit value from Planck 2015 [6].

- The 'Pantheon' binned Type Ia SNe from Scolnic et al. (2018) [58], which measure the ratio D_L/D_{H_0}.

- A direct Hubble constant measurement, similar to the 2.4% determination from Riess et al. (2016) [56].

In this paper, we forecast results using the same posterior mean for H_0 as in Riess et al. (2016) [56], but with uncertainties of only 1%. The updated GP regression code is archived here [47] and can be found in the public repository: ⟳[1]. The recently released H_0 constraint in Riess et al. (2019) [55], after the completion of this work, is now at the level of 1.9% and continues to be discrepant with the CMB-inferred value (now at 4.4σ), further strengthening the approach taken here and conclusions reached in this paper.

Following J18, we infer the evolution of the dark energy ($\rho_{\mathrm{DE}}(z)$) and matter densities from the expansion rate, by assuming flatness and no new physics at last scattering. We also infer the dark energy equation of state through the energy conservation equation as $w(z) = -1 - \rho'_{\mathrm{DE}}/(3\rho_{\mathrm{DE}})$, where the prime denotes derivative with respect to $\ln(a)$.

The results of the forecast GP regression appear in Fig. 1, which shows that the median inference (blue) favors D_H values larger than the fiducial model for redshifts above $z \sim 1.5$ and smaller below. At $z = 0$, D_A begins significantly below the fiducial values, eventually meeting them at $z = z_*$. Such a transition in D_H arises from the need to satisfy the constraint on $D_A(z_*)$. In Fig. 1, we also show the constraints from J18 (orange) using the current 2.4% precision on H_0. The error bars on the GP inference are smaller at high redshift (where there are no constraints) despite the increased precision in the H_0 measurement. This is a feature of using GP as a prior. In GP regression the size of the error bars are tied to the size of the fluctuations away from the mean function (the fiducial cosmology) unless there is data to constrain it. As the increased precision on H_0 favors a significant deviation away from the fiducial cosmology, the error bars are larger at high redshift.

The forecast inference of the dark energy evolution is shown in the upper panel of Fig. 2 and shows a transition in $w(z)$ that corresponds to the one in $D_H(z)$. Here, the GP regression picks out a median value for $w(0)$ greater than -1 and, interestingly, the median inference quickly transitions to values much less than -1. This $w(z)$ behavior is consistent with that found necessary to reconcile current cosmic shear and Planck CMB temperature measurements [41].

To understand why such an evolution in the dark energy component is preferred by the forecast data, note that the physical matter density at $z = 0$ is set by the constraint on $D_H(z_*)$ (see J18 for discussion). With this information known, the physical dark energy density at $z = 0$ is then set by the large value of H_0. In the case of a cosmological constant, the inferred matter and dark energy density would make $D_H(z)$ too small to explain the observed value of $D_A(z_*)$. Thus, in some interval between redshift zero and z_*, D_H needs to be increased, and this can be only achieved by allowing the dark energy component to evolve. The other datasets constrain the redshift dependence of dark energy. For example, the SNe constrain the shape of $D_H(z)$ and hence how fast the dark energy can evolve at low redshifts, which explains why the evolution starts above $z = 1$.

---

[1] https://github.com/rekeeley/GPHistTDE
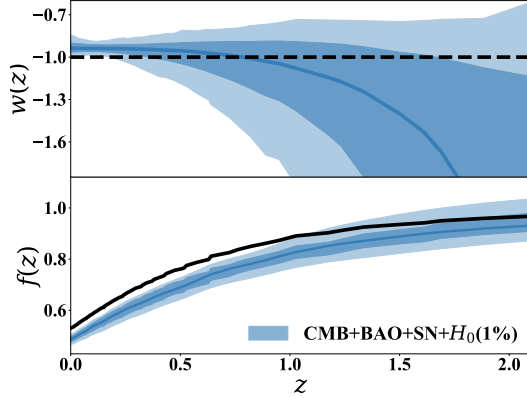
Figure 2. The top panel of the figure shows the inferred dark energy equation of state as a function of redshift from the GP regression. The bottom panel shows the growth rate $f = d\ln(D)/d\ln(a)$ from the GP regression. As in Fig. 1, the blue shaded regions correspond to the 68% and 95% confidence levels and the solid line corresponds to the median of the GP inference. The black solid line in the bottom panel corresponds to the ΛCDM growth rate.
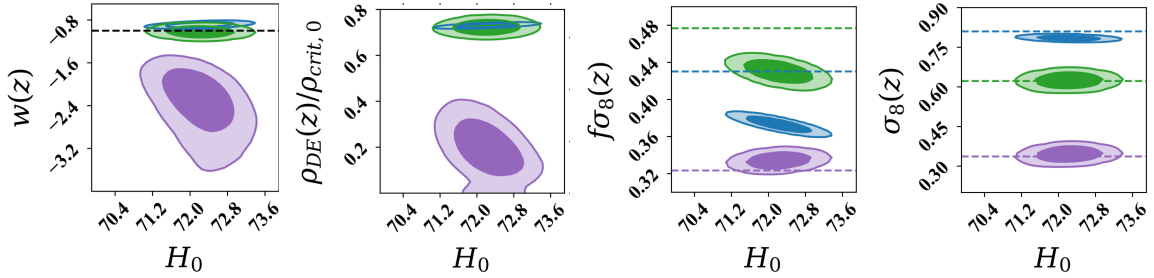
Figure 3. Posteriors of H_0 and representative derived parameters from the MCMC inference of the TDE model (inner 68% CL, outer 95% CL), fitting the same datasets as the GP. Each of these panels show the derived parameter evaluated at $z = 0$, $z = 0.5$, and $z = 2$ (blue, green, violet). These representative parameters are the equation of state (left), dark energy density scaled to the present critical density (center left), $f\sigma_8$ (center right), and σ_8 (right). The dashed horizontal lines correspond to the fiducial ΛCDM values for $w(z)$ $f\sigma_8(z)$ and $\sigma_8(z)$.

The growth history is inferred in the same manner as in J18, by solving the following differential equation:

$$\phi'' + (4 + H'/H)\phi' + (3 + 2H'/H)\phi = 0, \tag{2.2}$$

where ϕ is the gravitational potential. This equation can be derived from the spatial part of the perturbed Einstein equations in the conformal Newtonian gauge [51] by setting $\delta T^i_j = 0$, i.e., no shear or pressure perturbations. Another way to derive this equation is to use the covariant conservation of the energy momentum tensor [51], with the Poisson equation for ϕ on sub-horizon scales, and setting the two metric potentials (ϕ in the space-space part and ψ in the time-time part of the metric) equal to each other and pressure perturbations to zero.

For a cosmology with pressure-less matter and a cosmological constant, Eq. 2.2 is the same as the usual growth equation $\ddot{\delta}_m + 2H\dot{\delta}_m - 4\pi G\rho_m\delta_m = 0$ on sub-horizon scales, where $\rho_m\delta_m$ is the perturbation to the matter density and overdot denotes derivative with respect to coordinate time. Eq. 2.2 is a good way to explore modifications of the expansion history because early on ($z \gtrsim 2$) data prefers a matter-dominated cosmology and at late times

($z \lesssim 0.5$) data prefers dark energy with $w \simeq -1$. In making this assessment, we are implicitly assuming that the effective Gravitational constant appearing in the Poisson equation for the metric potential ψ is the same as the Newtonian one and that the gravitational "slip" [17, 23] is negligible on small scales (i.e., $\phi/\psi = 1$). Our results later indicate that a gravitational slip is not required to match the observed growth history.

We define the growth function $D = a\phi$ and the growth rate $f = D'/D$. In Fig. 2, we show how the inferred expansion history, which is significantly different from the fiducial ΛCDM expansion history, causes the corresponding growth history to differ from the fiducial ΛCDM expectation. The key result to note is that for $z < 1$, the expansion rate $H(z)$ is larger than the fiducial expansion rate and hence the growth of perturbations is slower. This demonstrates that the H_0 and σ_8 tensions could have a common origin.

We have not provided a concrete model for the preferred dark energy evolution and the growth rate encapsulated in Eq. 2.2. An interesting avenue to pursue is extensions to General Relativity (GR) that can motivate the kind of dark energy evolution that we have inferred. One such example is a new "Galileon" degree of freedom [29], which under the right initial conditions could have a dark energy equation of state $w = -2$ at high redshift and evolve towards $w = -1$ at low redshift, due to a de Sitter fixed point [44]. Such a $w(z)$ evolution is broadly consistent with our results but there is more growth than predicted by Eq. 2.2. There are also Generalized Proca theories (vector-tensor theories) with three propagating degrees of freedom where the early universe $w(z)$ could be $-1 - s$ with a late Universe de Sitter attractor [27, 34]. However, s is constrained from cosmological data (expansion history and growth) to be around 0.2 [28] and hence not consistent with solving the H_0 tension.

3   Transitional Dark Energy model
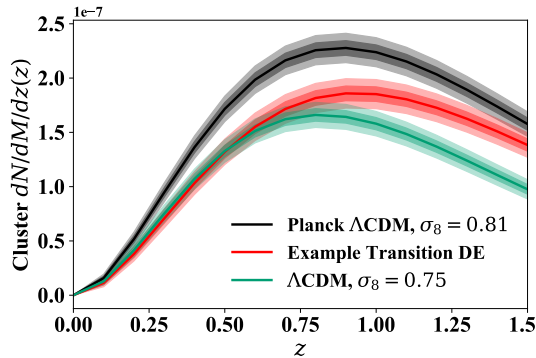
Figure 4. Sunyaev-Zel'dovich cluster counts $dN/dM/dz$ for a ΛCDM model consistent with Planck (black), a ΛCDM model with $\sigma_8 = 0.75$ (green), and an example TDE model (red). The shaded bands correspond to the cosmic variance 68% and 95% CLs.

To further investigate the implications of a rapid change in the dark energy density, we switch to a concrete parameterization of the dark energy evolution. This allows us to compute observables that are sensitive to the growth history, such as SZ cluster counts [8] using the cosmological Boltzmann solver CLASS [21], which was modified to allow for a rapid transition in the dark energy equation of state.

To this end, we define the TDE model as,

$$\rho_{\rm DE}(z) = \rho_{\rm DE,0}(1+z)^{3(1+W(z))},$$

$$W(z) = ((w_0 + w_1) + (w_1 - w_0)\tanh((z - z_t)/\Delta_z))/2,$$

(3.1)

where $W(z)$ is related to the equation of state,

$$W(z) = \frac{1}{\ln(1+z)} \int_{1/(1+z)}^{1} w(a)\frac{da}{a}.$$

(3.2)

This function is equivalent to the equation of state $w(z)$ in the regimes where $w(z)$ is constant. The equation of state tends towards w_0 at $z < z_t$ and towards w_1 at $z > z_t$. The width of this transition is parametrized by Δ_z. The values that fit the *median* GP inference are $w_0 = -0.95$, $w_1 = -1.95$, $z_t = 2.5$, and $\Delta_z = 0.9$. These values are used to calculate the growth functions in CLASS. Effectively, at early times the dark energy component is completely absent and then rapidly turns on by around redshift of 1. Similar models have been explored in the past [14, 59].

We performed a Markov Chain Monte Carlo (MCMC) analysis to sample the forecast posterior for the TDE model. We used the same datasets as in the forecast GP analysis, and varied all of the parameters of the TDE model (h, $\omega_{\rm m}$, w_0, w_1, Δ_z, z_T) in the MCMC. In Fig. 3, we show the forecast posteriors of the derived parameters $w(z)$, $\rho_{\rm DE}(z)/\rho_{\rm crit,0}$, $\sigma_8(z)$, and $f\sigma_8(z)$ for redshifts $z = 0, 0.5, 2$. These forecast posteriors illustrate that the datasets considered indeed would favor a drastic change in the dark energy equation of state at intermediate redshift, with little to no dark energy at $z = 2$ and a relatively sharp transition in the redshift range 0.5 to 2. We compute the Bayes factor (K) between the TDE model and the ΛCDM model and find $\ln K = 6.8$ in favor of the TDE model, corresponding to odds of 900 to 1 and 'decisive' preference for the TDE model when using Jeffreys' scale [39, 45]. A corresponding preference is found when computing the Deviance information criterion (DIC [61]), with ΔDIC = 24.2.

The correlations shown in the forecast posteriors are particularly interesting. The fact that large values of H_0 are correlated with smaller amounts of dark energy (or equivalently, more negative values of the equation of state) at $z = 2$ favors the idea that in order explain the observed value of $H_0 = 73\,{\rm km\,s^{-1}\,Mpc^{-1}}$, along with all of the other considered datasets, dark energy must be evolving in some form [30, 41, 67]. Moreover, as larger values of H_0 are correlated with less growth at $z < 2$ (most notably in $f\sigma_8$), this resolution to the H_0 problem would have interesting consequences for the σ_8 tension. When using the 2.4% uncertainty on H_0 from Riess et al. (2016) [56] instead of the projected 1% uncertainty, the posteriors for the TDE model become consistent with a cosmological constant (as in the GP regression from J18) and the global fit favors a value of H_0 around 69 ${\rm km\,s^{-1}\,Mpc^{-1}}$.

In Sec. B of the Appendix, we check that the TDE model can reproduce the best-fit ΛCDM C_ℓs by plotting the best-fit TDE parameters from a fit to the full Planck 2018 likelihoods [10]. Fig. 7 shows the C_ℓs from ΛCDM and TDE are identical above $\ell \sim 30$. The high ℓ agreement implies the best-fit ΛCDM and TDE models have the same values of θ_s and the diffusion damping scale, k_D, which further implies matching values for $D_H(z_*)$ and $D_A(z_*)$ for the best-fit ΛCDM and TDE models [43]. Thus, we can conclude that using ΛCDM-derived values for $D_H(z_*)$ and $D_A(z_*)$ for TDE inferences and GP inferences is self-consistent. It is likely the low ℓ disagreement arises from the late-time integrated Sachs-Wolfe effect and bears future study.

While the forecast TDE fitting and GP regression agree well on the preference for a transition in the dark energy evolution, the two methods show some differences in the details of the evolution. The GP inference allows for negative dark energy and so it has greater flexibility to fit both high and low-redshift data. By contrast, the dark energy density in the TDE model is constrained to be positive. Thus, in order to fit the CMB's D_A, the fit favors a transition in D_H that is sharper and at lower redshift than the transition in the median of the GP inference (see Figs. 1 and 10).

Using CLASS, we calculate the various measures of the growth of perturbations, such as the matter power spectra and $\sigma(R, z)$. We also compare the growth function from CLASS with the less model-dependent solution to Eq. 2.2 in the Appendix. The TDE model can change σ_8 through the clustering of dark energy (depending on the microphysics) and the change in the growth function due to the modified expansion history [32]. We assume that the dark energy density does not cluster significantly and, in keeping with this assumption, we keep the primordial power spectrum and transfer function fixed to that in ΛCDM but calculate the growth function at late times from our TDE dark energy model using CLASS.

The resulting inferences of $f\sigma_8$ and σ_8 at $z = \{0, 0.5, 2\}$ are shown in Fig. 3. Relative to the ΛCDM expectation, we find a noticeably slower growth rate today and at $z = 0.5$ ($\Delta f\sigma_8 \simeq 0.05$ for both redshifts), and mildly larger at $z = 2$ (by approximately 1–2σ). We also find that σ_8 at present is smaller in the preferred TDE model, at mild significance ($\simeq 2\sigma$). The predictions from the TDE model are consistent with the current measurements of $f\sigma_8$ at $z \lesssim 2$ [10]. The differences from the ΛCDM predictions for $f\sigma_8$ are small compared to the uncertainties in current growth rate measurements but measurable by future surveys [9, 12, 26, 38, 54, 60, 63].

4 SZ cluster abundance

As a concrete test of the observable differences between the TDE model and ΛCDM, we focus on the SZ cluster abundance. Using $\sigma(R, z)$ for the ΛCDM and TDE models, we can calculate the expected number density per unit mass of gravitationally collapsed objects,

$$\frac{dN}{dMdV}(M, z) = -\frac{\rho}{M^2} f_m(\sigma(M, z)) \frac{d\ln\sigma}{d\ln M}, \tag{4.1}$$

where N is the number of clusters in some volume V, M is the mass of the clusters, and ρ is the matter density. The multiplicity function $f_m(\sigma(M, z))$ is determined by fitting $dN/dV/dM$ to large volume N-body simulations, and we use the fitting function from Tinker et al. (2008) [64].

The number of clusters per unit mass per redshift is

$$\frac{dN}{dMdz} = \frac{dN}{dMdV} \frac{dV}{dz}, \tag{4.2}$$

where $dV/dz = 4\pi D_C^2 D_H$. We evaluate these functions at masses that for the two cosmologies give the same values of the SZ flux Y_{500}. Using the $M_{500} - Y_{500}$ relation from [8], we use $5 \times 10^{14} M_\odot$ for the ΛCDM case and $4.5 \times 10^{14} M_\odot$ (the redshift dependence of the relation is averaged over the redshift window where the SZ clusters are observed $0 < z < 0.4$) for the TDE case. The results of this calculation are shown in Fig. 4. There are two main sources of differences in the expected number of clusters in a redshift survey between ΛCDM and TDE models. One is in the multiplicity function through the dependence of $\sigma(R, z)$ on the TDE
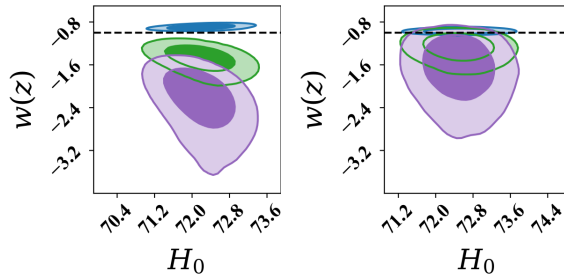
Figure 5. Posteriors of H_0 and $w(z)$ for $z = 0, 0.5, 2.0$ (blue, green violet) for the cases where $r_{\rm drag}$ is varied independently (left) and scaled linearly with $D_H(z_*)$ (right). The black dashed line corresponds to the ΛCDM equation of state $w = -1$.

parameters and the other is in dV/dz through the distances. We find that $f_m(\sigma(M, z))$ is smaller for the TDE model by 2–10% between $z = 1$ and $z = 0$. For the volumetric factor, the TDE model predicts a roughly 15–30% reduction in cluster counts between $z = 1.5$ and $z = 0$. Together, the smaller volumetric factor and smaller growth factors work to suppress the number of clusters relative to ΛCDM by 15–40% at these redshifts.

For tomographic cosmic shear measurements, similar considerations will apply and we expect the angular power spectra to be suppressed. We leave the potential of weak lensing and redshift space distortions to test these models for future work.

5 Internal consistency of low-z distance measurements

Recent work [13] has highlighted the tension between the BAO distances, calibrated to the value of $r_{\rm drag}$ from the ΛCDM fit to the Planck data, and the SN distances, calibrated to H_0. This tension is also present in our analysis. A possible resolution [13] is that $r_{\rm drag}$ is smaller than the value inferred for ΛCDM from Planck, but here we have assumed that there is no new physics at $z > 1000$ and hence $r_{\rm drag}$ is unchanged.

In this section, we report on results when deviating from our main analysis in two ways. Fig. 5 summarizes these results. In the first test, we allow $r_{\rm drag}$ to vary independently of other distances and scale BAO distances accordingly. A transition in the DE density between $z = 2$ and today is still inferred, but the equation of state varies more gently. The recovered value of $r_{\rm drag}$ is smaller, indicating the presence of a real tension between the BAO and SNe + H_0 datasets [13]. We discuss these points in greater detail with relevant plots in the Appendix.

In the second test, we allow $r_{\rm drag} \propto D_H(z_*)$ as an illustrative example to explore the degeneracy between new physics at early ($z > 1000$) and late times ($z < 3$). We allow the errors on $D_H(z_*)$ and $D_A(z_*)$ to be larger (TT+TE+EE+lowP constraints on ΛCDM + $N_{\rm eff}$ model in J18), as would be expected with the addition of new parameters. The inferred errors on the dark energy evolution are larger and it is not possible to reach a strong conclusion about the DE density at $z = 2$, although a sharp transition in the TDE equation of state is still allowed.

6 Conclusions

We performed a GP regression for the expansion history of the Universe using Planck measurements of the CMB, BOSS measurements of the BAO signal in the Lyα forest and LRGs,

Pantheon compilation of Type Ia SNe, and a measurement of the present Hubble parameter with forecasted 1% uncertainty. The forecast regression prefers a dark energy component with equation of state $w > -1$ at present, and has the density transition to zero by $z \simeq 2$. An interesting corollary of our result is the wide range of possibilities for the equation of state in the future, with a de Sitter phase not being favored. We calculated the growth history assuming no extra sources of clustering except for matter, and showed that the inferred growth rate in this model is measurably different from the Planck ΛCDM expectation.

Our forecast GP results are recovered when using a parametric model for dark energy evolution that allows for a sharp transition in the dark energy density. We used `CLASS` to calculate the predictions of this TDE model for SZ cluster counts and found that the TDE model predicts noticeably less SZ clusters than the best-fit ΛCDM model, potentially alleviating the σ_8 tension.

Similar, but less sharp, results were found when we allowed r_{drag} to vary independently of the CMB distances to explore the internal consistency between the $z < 1$ distance measurements. However, when r_{drag} was taken to scale linearly with $D_H(z_*)$ as an illustrative example of new physics at $z > 1000$, an evolving dark energy component was still allowed but not strongly preferred. In this case, the low-redshift distances agree better but that comes at the cost of not fitting the CMB precisely.

Direct reconstruction of the Universe's expansion history via the BAO signal that will be observed by future surveys, such as DESI, LSST, WFIRST, and Euclid should be able to robustly detect a transition in the dark energy equation of state. The fact that the TDE model predicts less growth of perturbations than ΛCDM offers another way to test this model through redshift space distortion measurements and tomographic weak lensing analysis in the future.

Our results suggest that a sharp transition in the dark energy equation of state for $1 < z < 2$ could simultaneously explain the H_0 and σ_8 tensions.

7 Acknowledgments

References

[1] B. P. Abbott et al. Gravitational Waves and Gamma-rays from a Binary Neutron Star Merger: GW170817 and GRB 170817A. *Astrophys. J.*, 848(2):L13, 2017.

[2] T. M. C. Abbott et al. Dark Energy Survey year 1 results: Cosmological constraints from galaxy clustering and weak lensing. *Phys. Rev.*, D98(4):043526, 2018.

[3] R. Adam et al. Planck 2015 results. I. Overview of products and scientific results. *Astron. Astrophys.*, 594:A1, 2016.

[4] P. A. R. Ade et al. Planck 2013 results. XVI. Cosmological parameters. *Astron. Astrophys.*, 571:A16, 2014.

[5] P. A. R. Ade et al. Planck 2013 results. XX. Cosmology from SunyaevZeldovich cluster counts. *Astron. Astrophys.*, 571:A20, 2014.

[6] P. A. R. Ade et al. Planck 2015 results. XIII. Cosmological parameters. *Astron. Astrophys.*, 594:A13, 2016.

[7] P. A. R. Ade et al. Planck 2015 results. XXIV. Cosmology from Sunyaev-Zeldovich cluster counts. *Astron. Astrophys.*, 594:A24, 2016.

[8] P. A. R. Ade et al. Planck 2015 results. XXIV. Cosmology from Sunyaev-Zeldovich cluster counts. *Astron. Astrophys.*, 594:A24, 2016.

[9] Amir Aghamousa et al. The DESI Experiment Part I: Science,Targeting, and Survey Design. 2016.

[10] N. Aghanim et al. Planck 2018 results. VI. Cosmological parameters. 2018.

[11] Shadab Alam et al. The clustering of galaxies in the completed SDSS-III Baryon Oscillation Spectroscopic Survey: cosmological analysis of the DR12 galaxy sample. *Mon. Not. Roy. Astron. Soc.*, 470(3):2617–2652, 2017.

[12] Luca Amendola et al. Cosmology and fundamental physics with the Euclid satellite. *Living Rev. Rel.*, 21(1):2, 2018.

[13] Kevin Aylor, MacKenzie Joy, Lloyd Knox, Marius Millea, Srinivasan Raghunathan, and W. L. Kimmy Wu. Sounds Discordant: Classical Distance Ladder & ΛCDM -based Determinations of the Cosmological Sound Horizon. 2018.

[14] Bruce A. Bassett, Martin Kunz, Joseph Silk, and Carlo Ungarelli. A Late time transition in the cosmic dark energy? *Mon. Not. Roy. Astron. Soc.*, 336:1217–1222, 2002.

[15] Rachael L. Beaton et al. The Carnegie-Chicago Hubble Program. I. An Independent Approach to the Extragalactic Distance Scale Using only Population II Distance Indicators. *Astrophys. J.*, 832(2):210, 2016.

[16] Jose Luis Bernal, Licia Verde, and Adam G. Riess. The trouble with H_0. *JCAP*, 1610(10):019, 2016.

[17] Edmund Bertschinger. On the Growth of Perturbations as a Test of Dark Energy. *Astrophys. J.*, 648:797–806, 2006.

[18] M. Betoule et al. Improved cosmological constraints from a joint analysis of the SDSS-II and SNLS supernova samples. *Astron. Astrophys.*, 568:A22, 2014.

[19] Florian Beutler et al. The clustering of galaxies in the completed SDSS-III Baryon Oscillation Spectroscopic Survey: Baryon Acoustic Oscillations in Fourier-space. *Submitted to: Mon. Not. Roy. Astron. Soc.*, 2016.

[20] S. Birrer et al. H0LiCOW - IX. Cosmographic analysis of the doubly imaged quasar SDSS 1206+4332 and a new measurement of the Hubble constant. *Mon. Not. Roy. Astron. Soc.*, 484:4726, 2019.

[21] D. Blas, J. Lesgourgues, and T. Tram. The Cosmic Linear Anisotropy Solving System (CLASS). Part II: Approximation schemes. *jcap*, 7:034, July 2011.

[22] S. Bocquet et al. Cluster Cosmology Constraints from the 2500 deg^2 SPT-SZ Survey: Inclusion of Weak Gravitational Lensing Data from Magellan and the Hubble Space Telescope. *Submitted to: Astrophys. J.*, 2018.

[23] Robert Caldwell, Asantha Cooray, and Alessandro Melchiorri. Constraints on a New Post-General Relativity Cosmological Parameter. *Phys. Rev.*, D76:023507, 2007.

[24] Hsin-Yu Chen, Maya Fishbach, and Daniel E. Holz. A 2 per cent Hubble constant measurement from standard sirens within 5 years. *Nature*, 562(7728):545–547, 2018.

[25] Michel Chevallier and David Polarski. Accelerating universes with scaling dark matter. *Int. J. Mod. Phys.*, D10:213–224, 2001.

[26] Kyle S. Dawson et al. The SDSS-IV extended Baryon Oscillation Spectroscopic Survey: Overview and Early Data. *Astron. J.*, 151:44, 2016.

[27] Antonio De Felice, Lavinia Heisenberg, Ryotaro Kase, Shinji Mukohyama, Shinji Tsujikawa, and Ying-li Zhang. Cosmology in generalized Proca theories. *JCAP*, 1606(06):048, 2016.

[28] Antonio de Felice, Lavinia Heisenberg, and Shinji Tsujikawa. Observational constraints on generalized Proca theories. *Phys. Rev.*, D95(12):123540, 2017.

[29] Antonio De Felice and Shinji Tsujikawa. Cosmology of a covariant Galileon field. *Phys. Rev. Lett.*, 105:111301, 2010.

[30] Eleonora Di Valentino, Alessandro Melchiorri, and Joseph Silk. Reconciling Planck with the local value of H_0 in extended parameter space. *Phys. Lett.*, B761:242–246, 2016.

[31] Hlion du Mas des Bourboux et al. Baryon acoustic oscillations from the complete SDSS-III Lyα-quasar cross-correlation function at $z = 2.4$. *Astron. Astrophys.*, 608:A130, 2017.

[32] Wenjuan Fang, Wayne Hu, and Antony Lewis. Crossing the Phantom Divide with Parameterized Post-Friedmann Dark Energy. *Phys. Rev.*, D78:087303, 2008.

[33] Wendy L. Freedman. Cosmology at a Crossroads. *Nat. Astron.*, 1:0121, 2017.

[34] Lavinia Heisenberg. Generalization of the Proca Action. *JCAP*, 1405:015, 2014.

[35] Catherine Heymans et al. CFHTLenS tomographic weak lensing cosmological parameter constraints: Mitigating the impact of intrinsic galaxy alignments. *Mon. Not. Roy. Astron. Soc.*, 432:2433, 2013.

[36] Chiaki Hikage et al. Cosmology from cosmic shear power spectra with Subaru Hyper Suprime-Cam first-year data. *Submitted to: Publ. Astron. Soc. Jap.*, 2018.

[37] H. Hildebrandt et al. KiDS-450: Cosmological parameter constraints from tomographic weak gravitational lensing. *Mon. Not. Roy. Astron. Soc.*, 465:1454, 2017.

[38] G. J. Hill et al. The Hobby-Eberly Telescope Dark Energy Experiment (HETDEX): Description and Early Pilot Survey Results. *ASP Conf. Ser.*, 399:115–118, 2008.

[39] Harold Jeffreys. *Theory of Probability*. Oxford University Press, Oxford, England, 3 edition, 1961.

[40] Shahab Joudaki et al. CFHTLenS revisited: assessing concordance with Planck including astrophysical systematics. *Mon. Not. Roy. Astron. Soc.*, 465(2):2033–2052, 2017.

[41] Shahab Joudaki et al. KiDS-450: Testing extensions to the standard cosmological model. *Mon. Not. Roy. Astron. Soc.*, 471:1259, 2017.

[42] Shahab Joudaki et al. KiDS-450 + 2dFLenS: Cosmological parameter constraints from weak gravitational lensing tomography and overlapping redshift-space galaxy clustering. *Mon. Not. Roy. Astron. Soc.*, 474(4):4894–4924, 2018.

[43] Shahab Joudaki, Manoj Kaplinghat, Ryan Keeley, and David Kirkby. Model independent inference of the expansion history and implications for the growth of structure. *Phys. Rev.*, D97(12):123501, 2018.

[44] Ryotaro Kase and Shinji Tsujikawa. Dark energy scenario consistent with GW170817 in theories beyond Horndeski gravity. *Phys. Rev.*, D97(10):103501, 2018.

[45] Robert E. Kass and Adrian E. Raftery. Bayes factors. *Journal of the American Statistical Association*, 90(430):773–795, 1995.

[46] David Kirkby and Ryan Keeley. Cosmological expansion history inference using gaussian processes, 2017.

[47] David Kirkby and Ryan Keeley. Cosmological expansion history inference with a 1% forecasted h0 measurement using gaussian processes, 2019.

[48] Christina D. Kreisch, Francis-Yan Cyr-Racine, and Olivier Dor. The Neutrino Puzzle: Anomalies, Interactions, and Cosmological Tensions. 2019.

[49] F. Khlinger et al. KiDS-450: The tomographic weak lensing power spectrum and constraints on cosmological parameters. *Mon. Not. Roy. Astron. Soc.*, 471(4):4412–4435, 2017.

[50] Eric V. Linder. Exploring the expansion history of the universe. *Phys. Rev. Lett.*, 90:091301, 2003.

[51] C.-P. Ma and E. Bertschinger. Cosmological Perturbation Theory in the Synchronous and Conformal Newtonian Gauges. *Astrophysical Journal*, 455:7, December 1995.

[52] Zhen Pan, Manoj Kaplinghat, and Lloyd Knox. Searching for Signatures of Dark matter-Dark Radiation Interaction in Observations of Large-scale Structure. *Phys. Rev.*, D97(10):103531, 2018.

[53] Vivian Poulin, Tristan L. Smith, Tanvi Karwal, and Marc Kamionkowski. Early Dark Energy Can Resolve The Hubble Tension. 2018.

[54] Johan Richard et al. 4MOST Consortium Survey 8: Cosmology Redshift Survey (CRS). *Messenger*, 175:50, 2019.

[55] Adam G. Riess, Stefano Casertano, Wenlong Yuan, Lucas M. Macri, and Dan Scolnic. Large Magellanic Cloud Cepheid Standards Provide a 1% Foundation for the Determination of the Hubble Constant and Stronger Evidence for Physics Beyond LambdaCDM. *arXiv e-prints*, page arXiv:1903.07603, Mar 2019.

[56] Adam G. Riess et al. A 2.4% Determination of the Local Value of the Hubble Constant. *Astrophys. J.*, 826(1):56, 2016.

[57] Adam G. Riess et al. New Parallaxes of Galactic Cepheids from Spatially Scanning the Hubble Space Telescope: Implications for the Hubble Constant. *Astrophysical Journal*, 855:136, March 2018.

[58] D. M. Scolnic et al. The Complete Light-curve Sample of Spectroscopically Confirmed SNe Ia from Pan-STARRS1 and Cosmological Constraints from the Combined Pantheon Sample. *Astrophys. J.*, 859(2):101, 2018.

[59] Arman Shafieloo, Varun Sahni, and Alexei A. Starobinsky. Is cosmic acceleration slowing down? *Phys. Rev.*, D80:101301, 2009.

[60] D. Spergel et al. Wide-Field InfrarRed Survey Telescope-Astrophysics Focused Telescope Assets WFIRST-AFTA 2015 Report. *arXiv e-prints*, page arXiv:1503.03757, Mar 2015.

[61] D. Spiegelhalter, N. G. Best, and B. P. Carlin. Bayesian measures of model complexity and fit. *J. Royal. Stat. Soc. B*, 64:583–639, October 2002.

[62] S. H. Suyu et al. The Hubble constant and new discoveries in cosmology. *ArXiv e-prints*, February 2012.

[63] Naoyuki Tamura et al. Prime Focus Spectrograph (PFS) for the Subaru Telescope: Overview, recent progress, and future perspectives. *Proc. SPIE Int. Soc. Opt. Eng.*, 9908:99081M, 2016.

[64] Jeremy L. Tinker, Andrey V. Kravtsov, Anatoly Klypin, Kevork Abazajian, Michael S. Warren, Gustavo Yepes, Stefan Gottlober, and Daniel E. Holz. Toward a halo mass function for precision cosmology: The Limits of universality. *Astrophys. J.*, 688:709–728, 2008.

[65] M. A. Troxel et al. Dark Energy Survey Year 1 results: Cosmological constraints from cosmic shear. *Phys. Rev.*, D98(4):043528, 2018.

[66] Edo van Uitert et al. KiDS+GAMA: cosmology constraints from a joint analysis of cosmic shear, galaxygalaxy lensing, and angular clustering. *Mon. Not. Roy. Astron. Soc.*, 476(4):4662–4689, 2018.
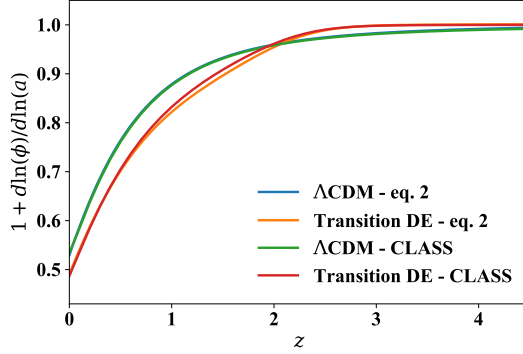
Figure 6. The growth rates for ΛCDM and TDE expansion histories, as calculated by Eq. 2.2 and as calculated by `CLASS`. The results from Eq. 2.2 for ΛCDM and TDE are in blue and orange, respectively. The results from `CLASS` for ΛCDM and TDE are in green and red, respectively.
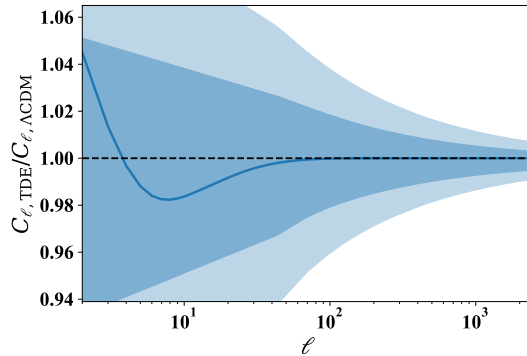
Figure 7. Ratio of C_ℓ for the temperature power spectra for a TDE model with best-fit parameters from the MCMC run (such that it predicts the ΛCDM values for $D_H(z_*)$ and $D_A(z_*)$) relative to the C_ℓ for the fiducial ΛCDM model. The bands correspond to the cosmic variance 68% and 95% CLs.

[67] Gong-Bo Zhao et al. Dynamical dark energy in light of the latest observations. *Nat. Astron.*, 1:627–632, 2017.

A   Growth rate calculation

Here we examine the consistency between the growth rate calculated from Eq. 2.2 and the growth rate extracted from `CLASS`. Specifically, we use the TDE parameters that match the median GP inference ($w_0 = -0.95$, $w_1 = -1.95$, $z_t = 2.5$, and $\Delta_z = 0.9$). Fig. 6 shows that in ΛCDM there is effectively no difference between the two methods to calculate the growth rate. For our TDE dark energy model there is a small but noticeable deviation at intermediate redshifts, in other words, at redshifts where the dark energy equation of state is varying rapidly. However, these deviations are much smaller than the difference from the ΛCDM growth rate.

B   Transitional Dark Energy model and the CMB

Here we investigate to what extent our proposed TDE model modifies the anisotropies in the CMB. To this end, we used `CLASS` to calculate the angular temperature power spectrum for

both the fiducial ΛCDM cosmology and a TDE model with best-fit parameters from a fit to the full Planck 2018 likelihoods [10]. As seen in Fig. 7, the C_ℓs of the best-fit parameters of these two models agree exactly for $\ell \gtrsim 30$. This implies the best-fit ΛCDM and TDE parameters yield the same values for θ_s and k_D. Hence, the best-fit TDE parameters yield $D_H(z_*) = 0.190$ Mpc (which effectively sets ω_m) and $D_A(z_*) = 12.6$ Mpc that match the ΛCDM values ($D_H(z_*) = 0.190$ Mpc and $D_A(z_*) = 12.6$ Mpc) [43]. Thus, it is self-consistent to use ΛCDM-derived values for TDE and GP inferences. In Figs. 8, 9 and 10, we show that the MCMC exploration of the TDE parameter space does result in the TDE model being tightly constrained around the ΛCDM values for $D_H(z_*)$ and $D_A(z_*)$. The discrepancies between TDE and ΛCDM C_ℓs at $\ell \lesssim 30$ is smaller than cosmic variance uncertainties and likely has implications for the late-time Sachs-Wolfe effect. We conclude that when the TDE model matches the ΛCDM values for $D_H(z_*)$ and $D_A(z_*)$, the C_ℓ cannot distinguish between the ΛCDM and TDE models.

C   Scaling the BAO distances

In this section of the Appendix, we explore the effects of allowing r_{drag} to vary on our inferences of the TDE model. The BAO distances scale with r_{drag} and if the value of r_{drag} that is preferred by a ΛCDM fit to the CMB is used for this scaling, the BAO distances disagree with the SN distances calibrated by the H_0 measurement [13], which is evident in Fig. 10. The TDE model alone cannot explain this discrepancy and only lowers its significance. Therefore, we investigate cosmologies where r_{drag} is allowed to vary.

We explore two cases, one where r_{drag} is allowed to vary independently of any other parameter, and another where it scales linearly with $D_H(z_*)$. The results for the first case are shown in Figs. 11–13. The most notable features of this case are that allowing r_{drag} to vary independently causes the low-redshift distances to completely agree (as expected), and also still shows a preference for little to no dark energy density at redshift $z = 2$. The evolution of the dark energy density between redshifts $z = 0$ and $z = 2$, however, is more gradual than the case where r_{drag} is fixed.

The Bayes factor for this model, relative to the ΛCDM model, is $\ln K = 7.9$ in favor of the TDE+r_{drag} model, or, relative to the TDE model, is $\ln K = 1.1$. This indicates no substantial preference, and that allowing the BAO distances to vary freely, on top of the TDE model, is only mildly preferred. Interestingly, there is moreover no preference for the ΛCDM+r_{drag} model over the ΛCDM-only model ($\ln K = -0.7$). This is because the preferred value of h in this case is around 0.7, and so the SN distances already agree with the BAO distances, thus leaving no work for the freely varying r_{drag} to perform.

The r_{drag} value inferred is smaller than the ΛCDM prediction by approximately 3%, which reflects the internal inconsistency between the $z < 1$ distances [13]. Whether this is due to an unknown systematic in the BAO distances or a signal for new physics that is relevant at $z > 1000$ is not evident.

When r_{drag} is tied to $D_H(z_*)$, a somewhat different picture emerges, as shown in Figs. 14–16. This scaling relationship is supposed to represent a more physically motivated way to vary r_{drag}. Such a scaling would arise if some variation left the sound speed of the pre-recombination plasma unchanged while causing the expansion history to scale up or down. This could happen, for example, if there is extra radiation or early dark energy [13, 16, 53]. To be self consistent, we also increased the error on $D_H(z_*)$ and $D_A(z_*)$ to be the same as that obtained from TT+TE+EE+lowP constraints in a ΛCDM + N_{eff} model (see Table I
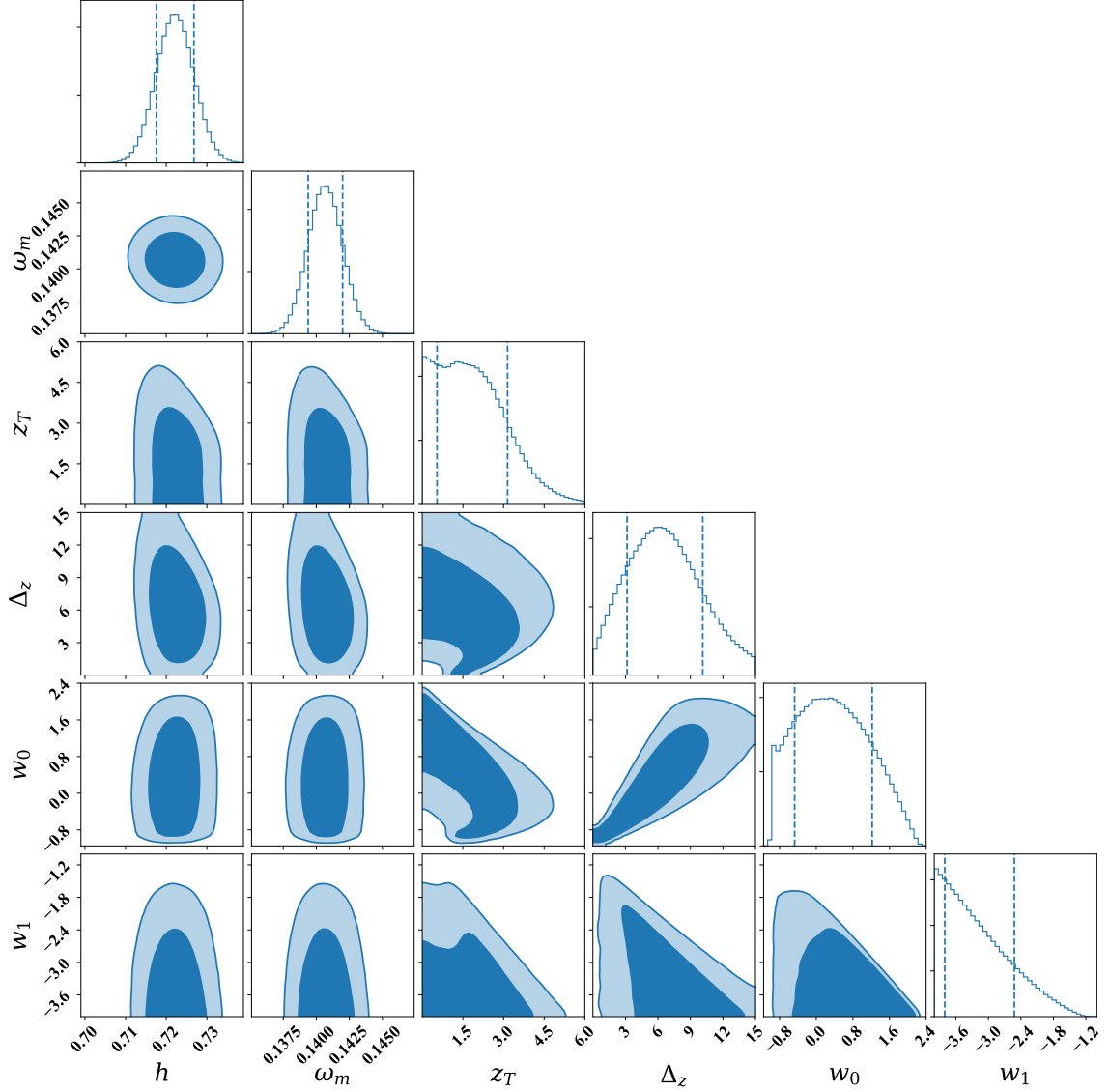
Figure 8. Posterior for an MCMC inference of the TDE model where z_T, Δ_z, w_0, and w_1 are varied, along with the ΛCDM parameters h and ω_m. The full dataset (CMB+Lyα+LRG+SN+H_0) from our GP analysis is being fit. Note the H_0 constraint here is the 1% projected error. For the 2D posteriors, the 68% and 95% CLs are shown in increasingly lighter shades of blue. For the 1D posteriors, the 68% CL is encapsulated by the dashed vertical lines. It is informative that this model can fit h and ω_m, the parameters that characterize both the low and high redshift anchors of the expansion history. It is less clear how to interpret the parameters that characterize the transition in the dark energy equation of state. Therefore we plot $\rho_{DE}(z)$ and $w(z)$ at various redshifts in Figs. 3 and 9 to show how these parameters work physically.
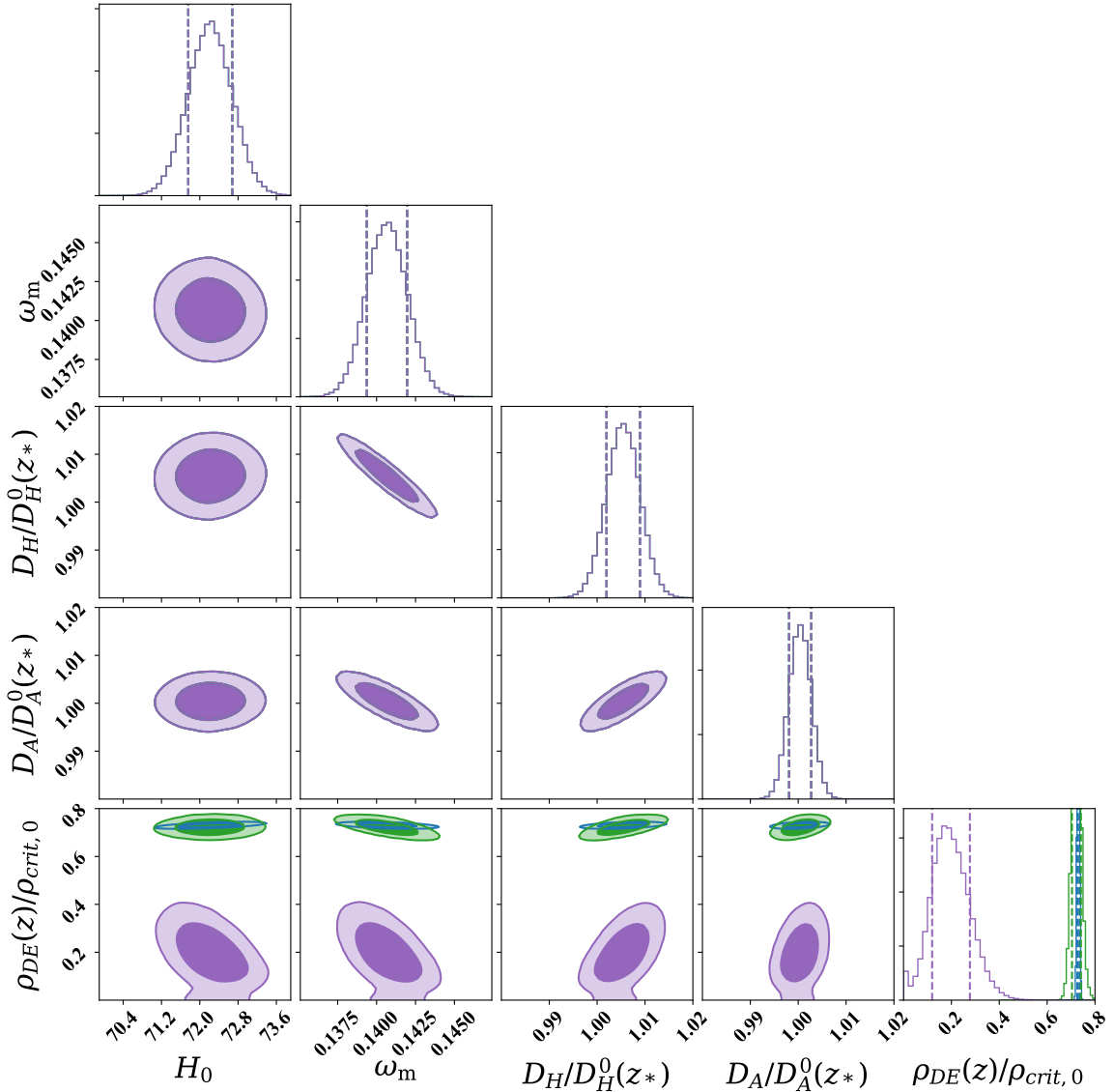
Figure 9. Same case as Fig. 8, except instead of the TDE parameters the quantities being displayed are the dark energy density at redshifts $z = 0, 0.5, 2.0$ (blue, green, violet) relative to the present value of the critical density, as well as $D_H(z_*)$ and $D_A(z_*)$ relative to the fiducial Planck 2015 values. These derived parameters are useful to show how inferences of the TDE model yield the same high redshift distances as ΛCDM, and to show how the dark energy density evolves physically.

in J18). If the size of the errors on $D_H(z_*)$ and $D_A(z_*)$ are obtained from the ΛCDM case, then the same results emerge, whether the $r_{\rm drag}$ is tied to $D_H(z_*)$ or fixed. In the ΛCDM $+ N_{\rm eff}$ case, the shifts in the distances relative to the ΛCDM values were not significant but the uncertainty increased by a factor of 3.

Using this more conservative constraint, we calculated the posterior for our TDE model where $r_{\rm drag}$ scales linearly with $D_H(z_*)$. This scaling shifts the whole distance ladder down by $\sim 5\%$ relative to the fiducial Planck ΛCDM values (see Fig. 16). No strong evidence for dark energy evolution was found, though such evolution remains allowed, as shown in
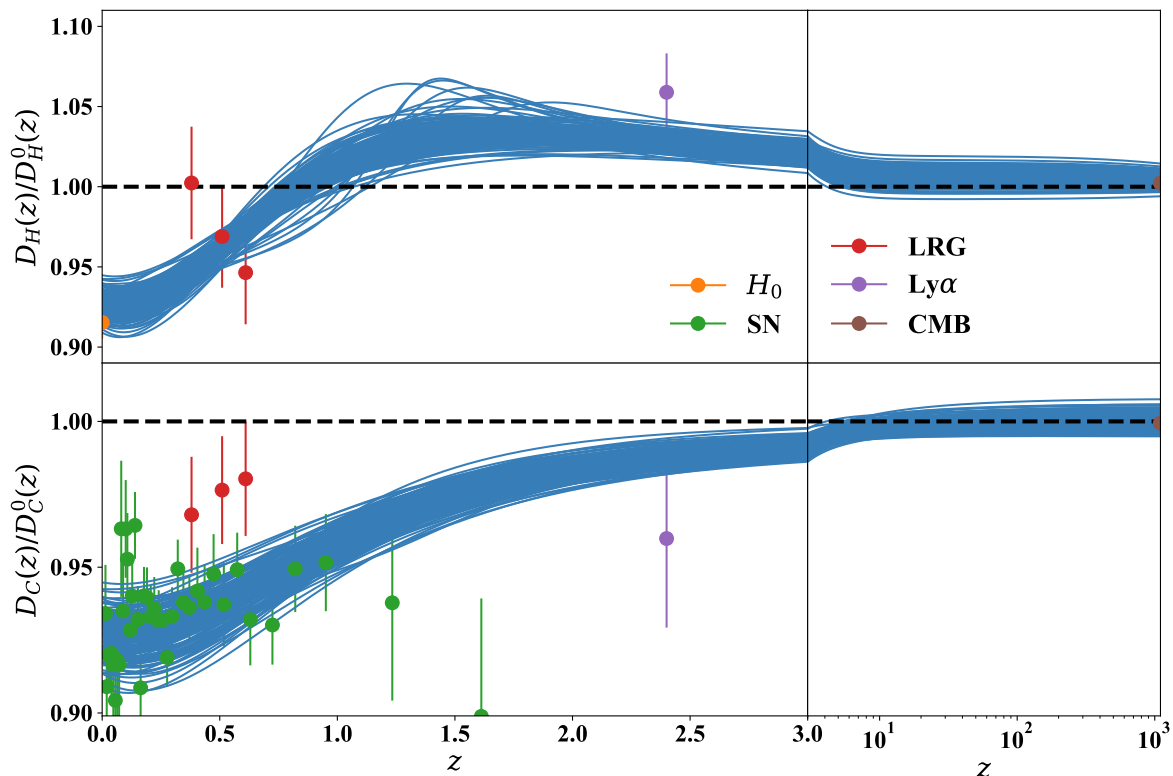
Figure 10. Posterior predictive distribution composed of sample expansion histories (blue) drawn from an MCMC sampling of the posterior of the TDE model as in Fig. 8. The spread in these expansion histories corresponds to the posterior uncertainty in the expansion history. The data are plotted in various colors, orange for H_0, green for the SNe data, red for the LRG data, violet for the Lyα data, and brown for the CMB data. The SNe constrain only the ratio of the distances D_L/D_{H_0} so the absolute scale of the SNe data points in this figure is set by the best fit H_0. Similarly, the BAO data points (LRG + Lyα) only constrain the ratios $D_H/r_{\rm drag}$, $D_A/r_{\rm drag}$ so the absolute scale for these distances is set by the best fit value from Planck 2015 [6], $r_{\rm drag} = 147$. These distances draw from the posterior are useful to demonstrate which features of the data are driving the need for a transition in the dark energy equation of state, primarily $D_A(z_*)$.

Fig. 15. The picture is essentially the same if $r_{\rm drag}$ scales as $D_H(z_*)^{1.5}$, which is the best-fit scaling relation calculated in J18 for the ΛCDM + $N_{\rm eff}$ model. The Bayes factor for the TDE model relative to ΛCDM, both with $r_{\rm drag}$ tied to $D_H(z_*)$, is $\ln K = -0.8$. This indicates no substantial preference between the TDE+$r_{\rm drag}$ and the ΛCDM+$r_{\rm drag}$ models.

The ability of the model where $r_{\rm drag}$ and $D_H(z_*)$ vary in tandem to alleviate the tensions in cosmological distances relies on the fact that the CMB constraint is less stringent. This can be seen in Fig. 16, where the preferred high redshift distances are pulled away from the centers of the CMB constraint, beyond the 1σ range. If the uncertainties in the constraint were reduced to their size in ΛCDM, then any preference for the BAO distances to be scaled to the values picked out by the SNe disappears, and the strong preference for the TDE reappears. Unless the BAO distances are disconnected from the CMB distances, there remains some degree of tension between the inferred distances, either at $z = 0$ in the ΛCDM model, at $z \sim 0.5$ in the TDE model, or at $z = z_*$ for the ΛCDM (or TDE) model wherein $r_{\rm drag}$ and $D_H(z_*)$ covary.
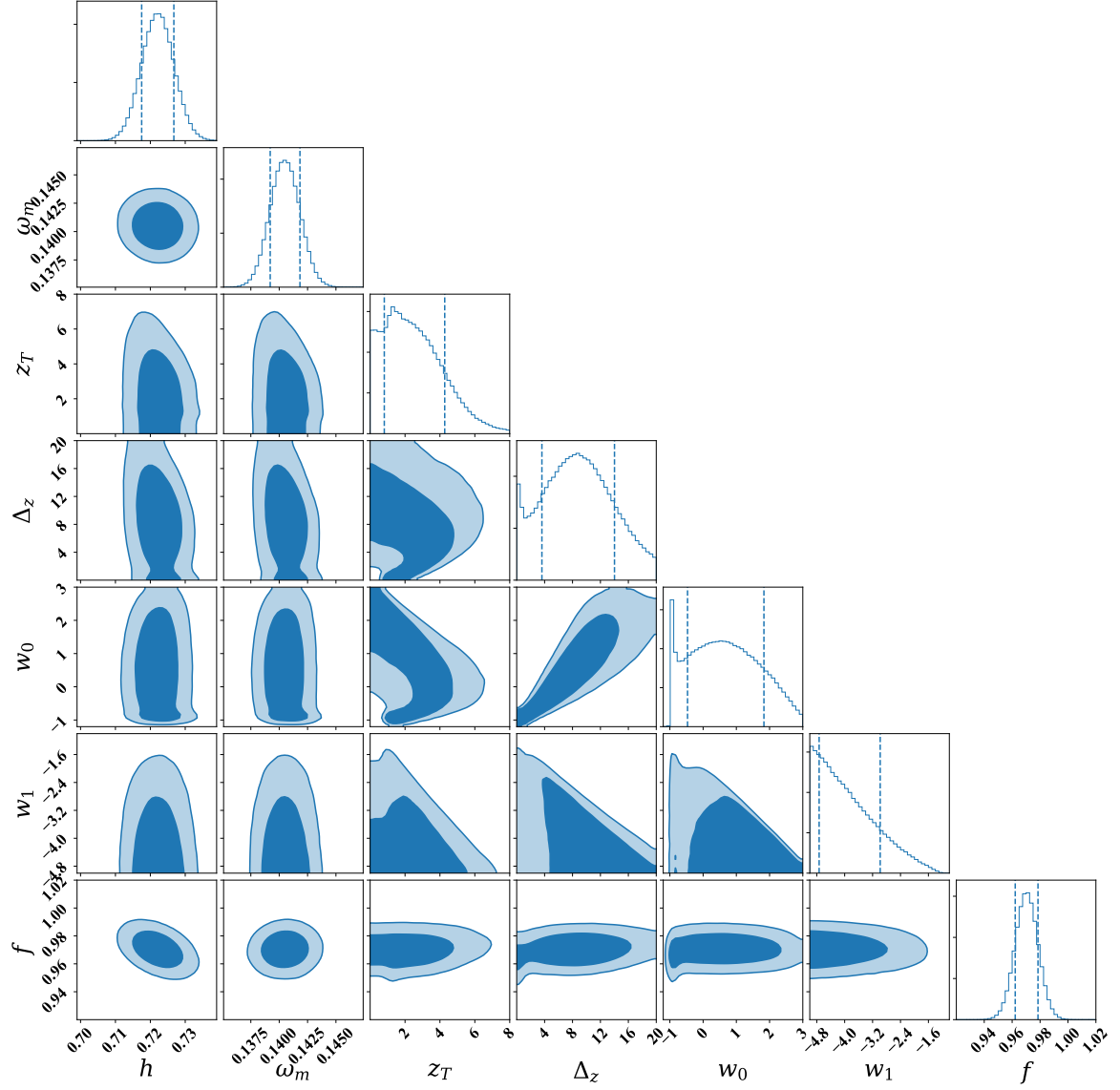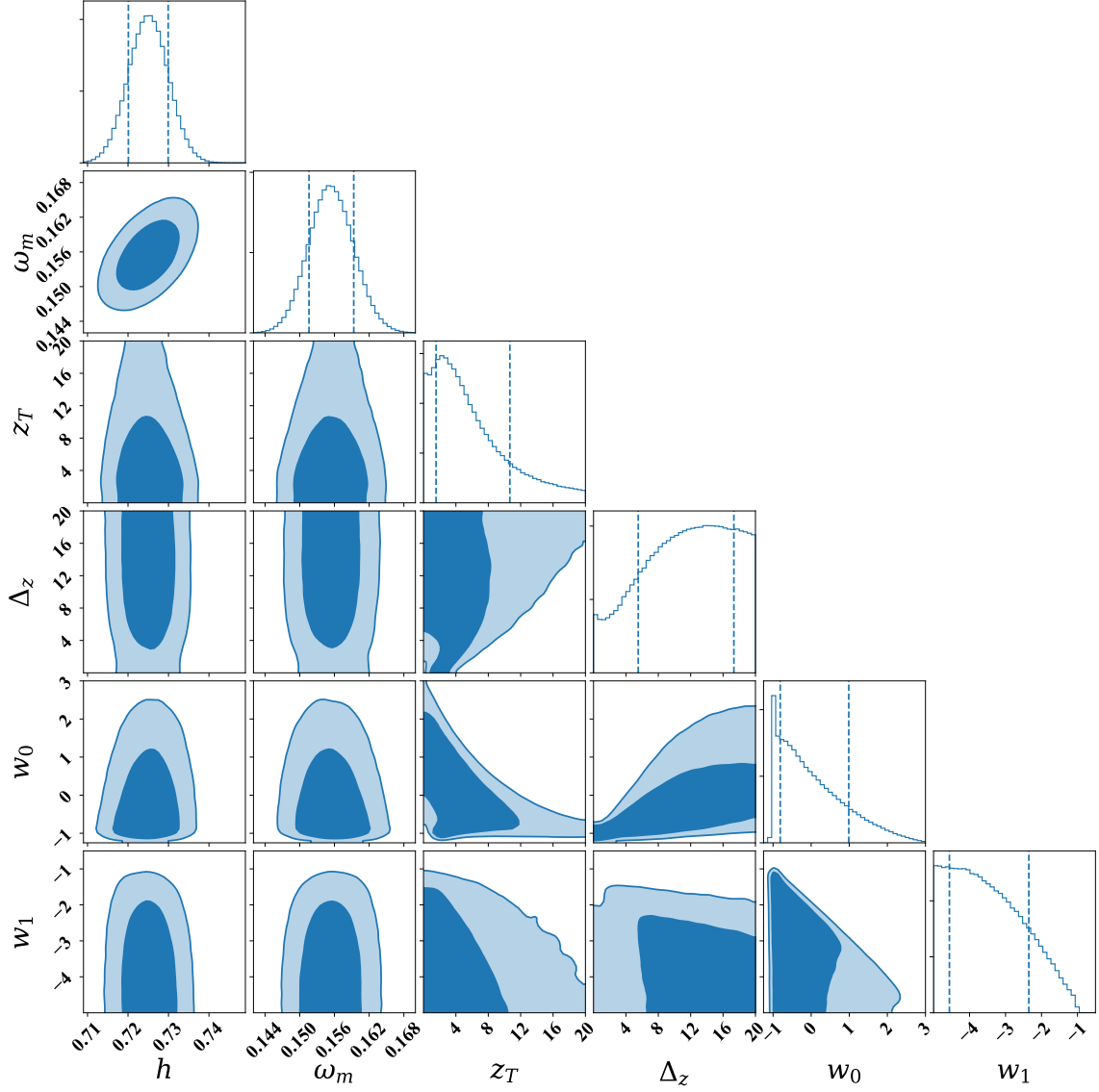
Figure 11. Posteriors for the TDE model but now r_{drag} is scaled by an extra parameter f. The fact f is noticeably below 1 shows the magnitude of the disagreement between the Planck-ΛCDM calibrated LRG distances and the H_0 calibrated SNe distances.
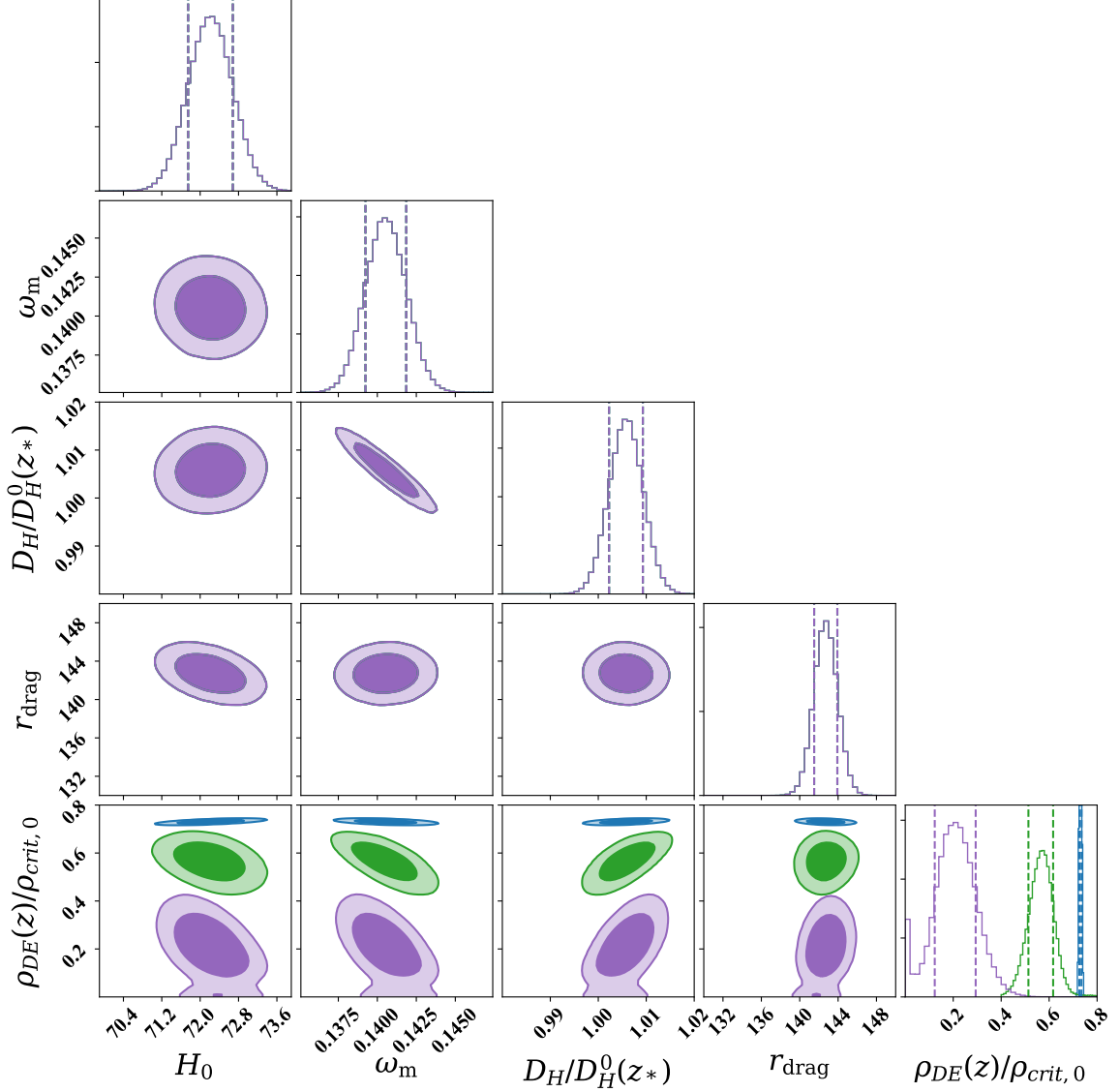
Figure 12. The same case as in Fig. 11 but shown are the posteriors for the derived parameters including $D_H(z_*)$, r_{drag}, and $\rho_{\mathrm{DE}}(z)/\rho_{\mathrm{crit},0}$, for redshifts $z = 0, 0.5, 2$ (blue, green, violet). As with Fig. 9, this figure shows how inferences of the TDE model yield the same values of $D_H(z_*)$ as ΛCDM, and shows how the dark energy density evolves physically. The r_{drag} posterior shows how it must be shifted to lower values than the ΛCDM value to get the LRG and SNe distances to agree.
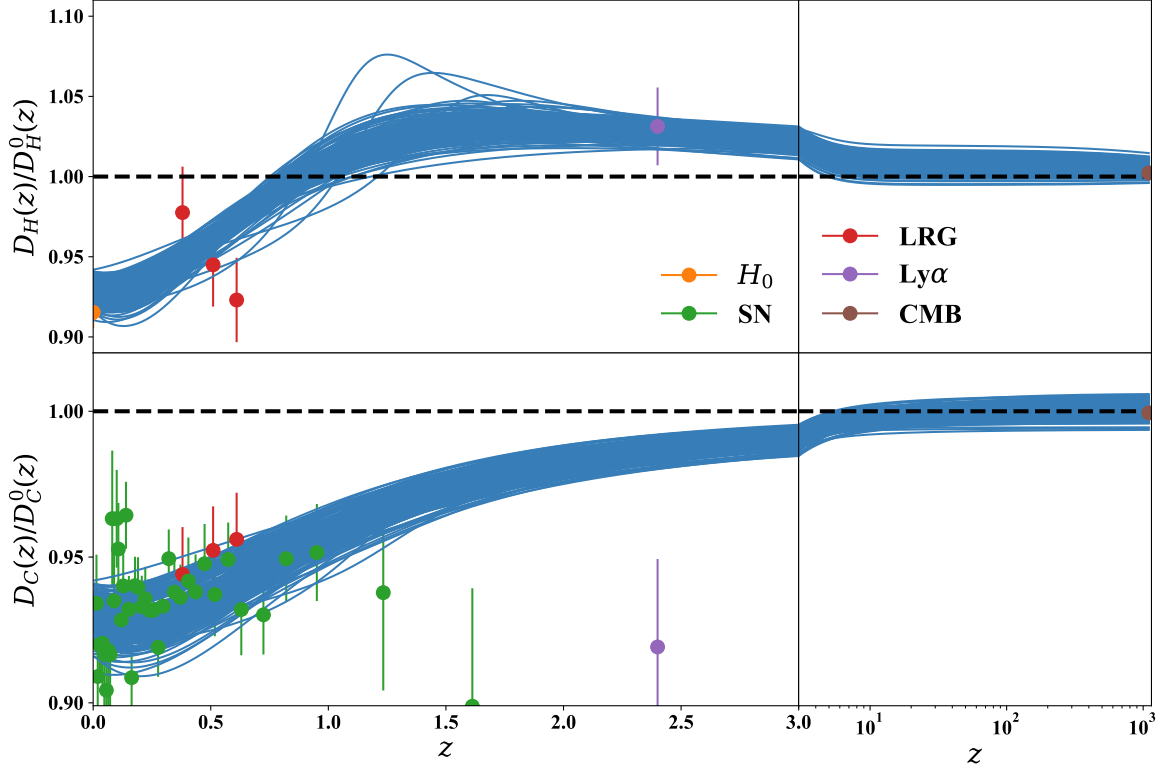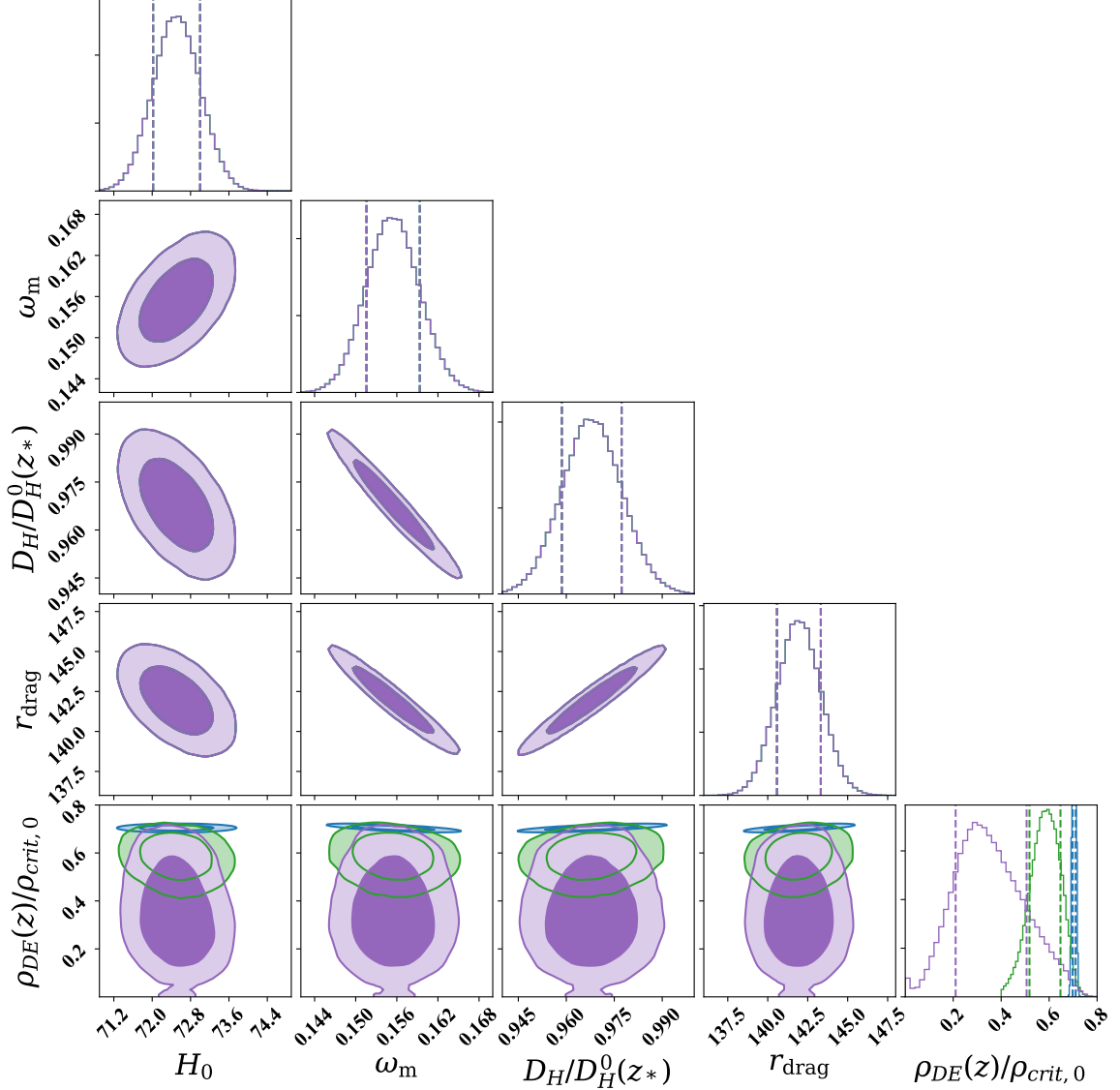
Figure 13. The same case as in Fig. 11 but shown is the posterior predictive distribution, as in Fig. 10. The absolute scale of the SNe data points are again set by the best fit value of H_0 while the absolute scale for the BAO data points are set by the best fit r_{drag}, which in this case, is allowed to vary freely. As with Fig. 10, these posterior-sampled distances are useful to demonstrate which features of the data are driving the need for a transition in the dark energy equation of state, primarily $D_A(z_*)$. The difference with Fig. 10 is that now r_{drag} is allowed to scale freely so the LRG and SNe distances agree.

Figure 14. Posteriors for the TDE model but now r_{drag} scales linearly with D_H. The derived values of ω_m are noticeably different than in Figs. 8 and 11 since the need to modify r_{drag} requires a corresponding change in ω_m.

Figure 15. The same case as in Fig. 14 but shown are the posteriors for the derived parameters including $D_H(z_*)$, r_{drag}, and $\rho_{\text{DE}}(z)/\rho_{\text{crit},0}$, for redshifts $z = 0, 0.5, 2$ (blue, green, violet). Similar to Figs. 9 and 12, this plots is useful to show how the TDE model with r_{drag} scaling linearly with $D_H(z_*)$ predicts values for ω_m, $D_H(z_*)$ and r_{drag} different than the ΛCDM values, while showing no strong preference for a transition in the dark energy density.
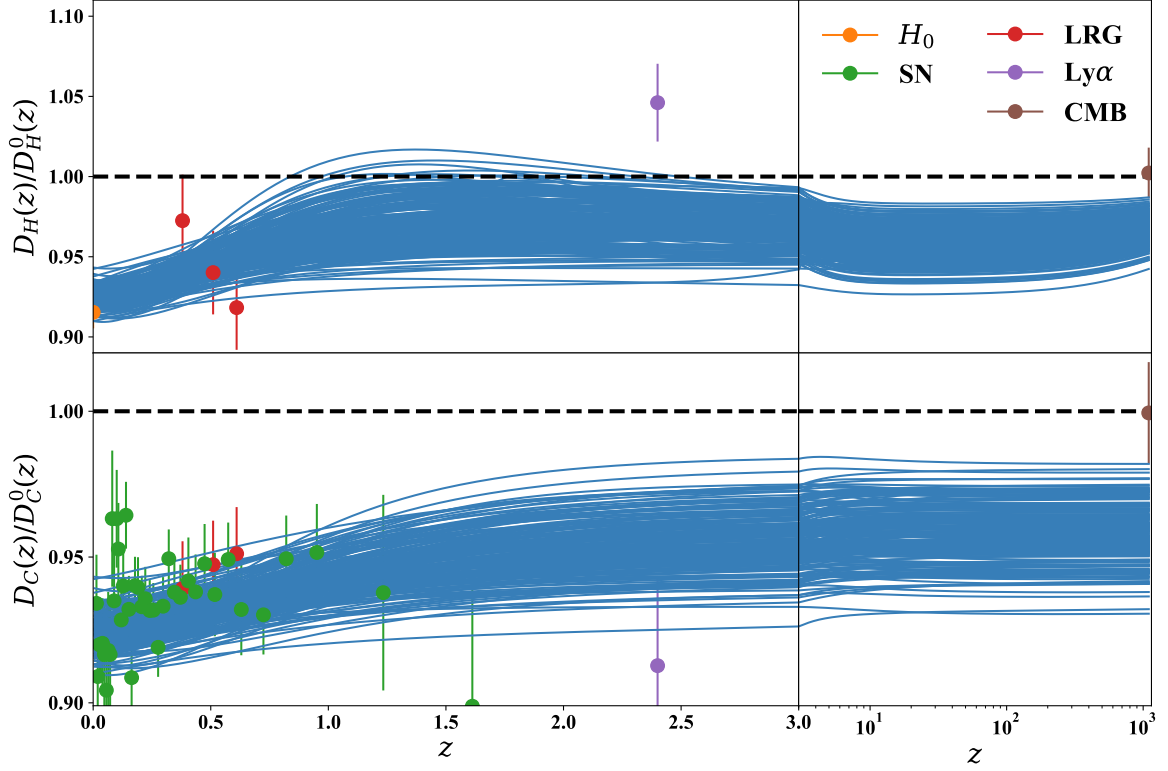
Figure 16. The same case as in Fig. 14 but shown is the posterior predictive distribution, as in Fig. 10. The absolute scale of the SNe are determined as in Fig. 10, while the absolute scale for the BAO data points are set by the best fit $r_{\rm drag}$, which in this case, varies linearly with $D_H(z_*)$. As with Figs. 10 and 13, this plot is useful in showing what features of the data are driving the results. The larger uncertainties on the CMB distances, combined with the preference to shift the LRG distances down to the SNe distances, shifts the whole expansion history down, rather than invoke a transitional dark energy density.